Title

Interfering RNA against PKC-Î± inhibits TNF-Î±-induced IP
3
R1 expression and improves glomerular filtration rate in rats with fulminant hepatic failure

Journal

American Journal of Physiology-Renal Physiology, 314(5)

ISSN

1931-857X 1522-1466

Authors

Wang, Dong-Lei
Dai, Wen-Ying
Wang, Wen
et al.

Publication Date

2018-05-01

DOI

10.1152/ajprenal.00433.2016

Data Availability

Associated data will be made available after this publication is published.

Peer reviewed

Am J Physiol Renal Physiol 314: F942–F955, 2018.
First published January 10, 2018; doi:10.1152/ajprenal.00433.2016.

RESEARCH ARTICLE | *Precision Medicine in Kidney Disease and Injury*

Interfering RNA against PKC-α inhibits TNF-α-induced IP_3R1 expression and improves glomerular filtration rate in rats with fulminant hepatic failure

Dong-Lei Wang,[1] Wen-Ying Dai,[2] Wen Wang,[1] Ying Wen,[1] Ying Zhou,[1] Yi-Tong Zhao,[2] Jian Wu,[3,4]* and Pei Liu[1,5]*

[1]*Department of Infectious Diseases, The First Affiliated Hospital, China Medical University, Shenyang City, Liaoning Province, People's Republic of China;* [2]*The Sixth People's Hospital of Shenyang, Shenyang City, Liaoning Province, People's Republic of China;* [3]*Department of Medical Microbiology, Key Laboratory of Medical Molecular Virology, School of Basic Medical Sciences, Fudan University, Shanghai, China;* [4]*Shanghai Institute of Liver Diseases, Fudan University, Shanghai, China; and* [5]*The Institute of liver diseases, China Medical University, Shenyang, Liaoning Province, China*

Submitted 4 August 2016; accepted in final form 4 January 2018

Wang DL, Dai WY, Wang W, Wen Y, Zhou Y, Zhao YT, Wu J, Liu P. Interfering RNA against PKC-α inhibits TNF-α-induced IP_3R1 expression and improves glomerular filtration rate in rats with fulminant hepatic failure. *Am J Physiol Renal Physiol* 314: F942–F955, 2018. First published January 10, 2018; doi:10.1152/ajprenal.00433.2016.—We have reported that tumor necrosis factor-α (TNF-α) is critical for reduction of glomerular filtration rate (GFR) in rats with fulminant hepatic failure (FHF). The present study aims to evaluate the underlying mechanisms of decreased GFR during acute hepatic failure. Rats with FHF induced by D-galactosamine plus lipopolysaccharide (GalN/LPS) were injected intravenously with recombinant lentivirus harboring short hairpin RNA against the protein kinase C-α (*PKC-α*) gene (Lenti-shRNA-PKC-α). GFR, serum levels of aminotransferases, creatinine, urea nitrogen, potassium, sodium, chloride, TNF-α, and endothelin-1 (ET-1), as well as type 1 inositol 1,4,5-trisphosphate receptor (IP_3R1) expression in renal tissue were assessed. The effects of *PKC-α* silencing on TNF-α-induced IP_3R1, specificity protein 1 (SP-1), and c-Jun NH_2-terminal kinase (JNK) expression, as well as cytosolic calcium content were determined in glomerular mesangial cell (GMCs) with RNAi against *PKC-α*. Renal IP_3R1 overexpression was abrogated by pre-treatment with Lenti-shRNA-PKC-α. The *PKC-α* silence significantly improved the compromised GFR, reduced Cr levels, and reversed the decrease in glomerular inulin space and the increase in glomerular calcium content in GalN/LPS-exposed rats. TNF-α treatment increased expression of PKC-α, IP_3R1, specificity protein 1 (SP-1), JNK, and p-JNK in GMCs and increased Ca^{2+} release and binding activity of SP-1 to the *IP₃R1* promoter. These effects were blocked by transfection of siRNA against the *PKC-α* gene, and the *PKC-α* gene silence also restored cytosolic Ca^{2+} concentration. RNAi targeting *PKC-α* inhibited TNF-α-induced IP_3R1 overexpression and in turn improved compromised GFR in the development of acute kidney injury during FHF in rats.

acute kidney failure; fulminant hepatic failure; protein kinase C-α; type 1 inositol 1,4,5-trisphosphate receptor; tumor necrosis factor-α

INTRODUCTION

Advanced hepatic failure is often accompanied with acute kidney injury (AKI) and has a poor prognosis due to the deterioration of both renal and liver function. Complex mechanisms are likely involved in renal malfunction during severe liver failure, such as alteration in systemic hemodynamics, subsequent renal hypoperfusion, activation of vasoconstrictor systems, and reduced activity of vasodilator systems (13). Ultimately, renal vasoconstriction leads to a pronounced reduction in the glomerular filtration rate (GFR) (3, 8). Glomerular mesangial cells (GMCs) regulate glomerular filtration pressure (GFP) by changing glomerular capillary filtration surface area through their contraction (22). Vascular smooth muscle cells (VSMCs) in preglomerular resistance vessels (interlobular artery and afferent arteriole) mediate constriction or dilation of the vessels (i.e., changes in luminal diameter), in turn regulating renal vascular resistance, renal blood flow, and GFR (2). Multifactorial mechanisms are involved in abnormal regulation of renal blood flow and GFR (24). Plasma levels of angiotensin II, endothelin-1 (ET-1), norepinephrine (NE), and tumor necrosis factor-α (TNF-α) are significantly increased in patients with severe liver injury (6, 23). Cytosolic Ca^{2+} concentration ($[Ca^{2+}]_i$) in GMCs and VSMCs responds to a couple of external signals and activates various effectors, including cellular contraction (21, 32). Growing evidence suggests that serum TNF-α levels are significantly increased in patients with severe liver injury; meanwhile, TNF-α inhibitors, such as pentoxifylline, reduce the incidence of renal failure and mortality of hepatic renal syndrome. Therefore, it is conceivable that TNF-α plays a crucial role in the development of renal failure during hepatic insufficiency (1).

Our previous study demonstrated that rats with fulminant hepatic failure (FHF) exhibited an increased level of serum creatinine (Cr) and enhanced expression of type 1 inositol 1,4,5-trisphosphate receptor (IP_3R1) protein. At the same time, these rats exhibited a similar trend of increased plasma TNF-α and ET-1 levels. Pretreatment with anti-TNF-α antibody significantly improved renal function and GFR (29). TNF-α treatment led to an increase in IP_3R1 expression; in turn, enhanced IP_3R1 expression amplified the sensitivity of GMCs and VSMCs in response to a variety of vasoconstrictors, thus leading to contraction of these two cell types and resulting in

* J. Wu and P. Liu contributed equally to this work.
Address for reprint requests and other correspondence: P. Liu, Dept. of Infectious Diseases and the Institute of Liver Diseases, The First Affiliated Hospital, China Medical Univ., 155 Nanjing North St., Shenyang 110001, Liaoning Province, China (e-mail: syliupei2013@163.com).

reduced GFR. Our previous findings indicated that TNF-α induced IP_3R1 expression in human mesangial cells through TNFR1/PC-PLC/PKC-α and TNFR2 signaling pathways (30). To further elucidate the role of PKC-α in the mediation of IP_3R1 expression and downstream effects, the present study was aimed at investigating the effects of blocking *PKC-α* by an RNAi approach on renal function and GFR in rats with FHF and acute renal failure. Furthermore, we investigated the TNF-α/PKC-α/IP_3R1 pathway in GMCs to identify target molecules that modulate the pathogenesis of FHF with AKI. Our findings point to a new direction of molecular intervention by directly targeting this novel pathway in severe liver failure with multiple-organ malfunction.

MATERIALS AND METHODS

Sources of materials. TNF-α, D-galactosamine hydrochloride (GalN), lipopolysaccharide (LPS), fluorescein isothiocyanate (FITC-inulin), and ET-1 were obtained from Sigma Chemical (St. Louis, MO). Micro-osmotic pumps at a release rate of 1.0 ml/h were purchased from Durect (Cupertino, CA). Other reagents were obtained as follows: polyclonal IP_3R1 antibody was from Synaptic Systems; SP-1 antibody, protein A agarose, and salmon sperm DNA were from Millipore (Billerica, MA); polyclonal PKC-α antibody was from BioWorld Technology (St. Louis Park, MN); JNK 1/2/3 polyclonal antibody was from ImmunoWay (Suzhou, Jiangsu, China); p-JNK antibody was from Cell Signaling Technology (Danvers, MA); β-actin and GAPDH antibody were from Proteintech Group (Rosemont, PA); goat horseradish peroxidase-conjugated anti-rat/mouse IgG was from Zhongshan Biotechnology (Beijing, China); Lipofectamine RNAiMAX reagent was from Invitrogen (Carlsbad, CA); SP600125 was from Beyotime Technology (Shanghai, China); lentivirus vectors were commissioned by GenePharma (Shanghai, China); and the rat NAG ELISA kit and rat microalbuminuria (MAU/ALB) kit were from Cusabio Life Science (Baltimore, MD).

Small interfering RNA target sequences. Small interfering RNAs (siRNAs) against *PKC-α* and control siRNA were designed by Invitrogen using siRNA software (Waltham, MA). The full-length *PKC-α* gene sequence was retrieved from GenBank (NM_001105713). Three pairs of siRNAs against the rat *PKC-α* gene were designed, and one was selected based on preliminary results. The siRNA sequences were as follows: 5′-GGUUCACAAGAGGUGCCAUTT-3′ (sense) and 5′-AUGGCACCUCUUGUGAACCTT-3′ (antisense). Universal negative control siRNA sequences were as follows: 5′-UUCUCCGAACGUGUCACGUTT-3′ (sense) and 5′-ACGUGACACGUUCGGAGAATT-3′ (antisense).

Short hairpin RNA (shRNA) against *PKC-α* was converted and synthesized by Genepharma designer based on our siRNA sequence used in the preliminary experiments. The sense sequences of effective *PKC-α* shRNA and negative control oligonucleotide (NC) were as follows: LV-PKC-α-shRNA: 5′-GGTTCACAAGAGGTGCCAT-3′ and LV-NC-shRNA: 5′-TTCTCCGAACGTGTCACGTTTC-3′.

Since siRNA is not stable in vivo and could not transfect nondividing cells and whole model organisms easily, we used an HIV-based lentivector expression construct instead of siRNA. Lentiviral expression vector (LV3-H1-GFP-Puro) was constructed by Genepharma. The packaging plasmids consist of optimized three plasmids: PG-P1-VSVG, PG-P2-REV, and PG-P3-RRE. 293T cells were cotransfected with lentiviral expression construct and packaging plasmids with Lipofectamine 2000. Transfected cells were changed with fresh complete DMEM medium 6 h after transfection and were cultured for another 72 h. Viral particles were collected, and viral transduction unit was determined by counting the number of cells positive for enhanced green fluorescent protein by fluorescent microscopy.

Animal model of FHF and in vivo transduction of lentiviral vector harboring shRNA against PKC-α. Our animal experimental procedures were approved by the animal ethic committee of the Chinese Medical University and followed the National Institutes of Health *Guide for the Care and Use of Laboratory Animals*. Male Sprague-Dawley rats weighing ~220 ± 20 g were housed in stainless steel mesh cages under controlled temperature (23 ± 3°C) and light illumination for 12 h daily. Animals were allowed free access to food and tap water throughout acclimatization for 1 wk and during an entire experimental period. Rats were injected through the tail vein with 1.0×10^8 transduction units of lentivirus harboring shRNA against the rat *PKC-α* gene. The timeline of animal experimental design is shown in Fig. 1*A*.

Preparation of FITC-inulin solution. FITC-inulin (24%) was dissolved in a 0.9% NaCl solution as described previously (18). To remove residual FITC unbound to inulin, the solution was dialyzed in 1,000 ml of 0.9% NaCl at room temperature for 24 h using a 1,000-Da cutoff dialysis membrane (Spectrum Laboratories, Rancho Dominguez, CA) in the dark and then sterilized by filtration through a 0.22-μm filter (18).

Implantation of micro-osmotic pumps. A total of 36 rats which received injection of lentiviruses harboring shRNA against PKC-α or control shRNA 1 wk before were implanted for micro-osmotic pumps. These rats were anesthetized with intraperitoneal injection of pentobarbital sodium (40 mg/kg). Two micro-osmotic pumps filled with 200 μl of 8% FITC-inulin were inserted into the peritoneal cavity 7 days before GalN/LPS administration. A pilot study revealed that plasma FITC levels were inadequate for measuring GFR when a single micro-osmotic pump was implanted. After two pumps were implanted, a two- to sixfold increase in plasma fluorescence levels was detected (18).

Induction of FHF and treatments in different groups. FHF was induced in rats using a combination of GalN (400 mg/kg) plus LPS (32 μg/kg) in saline, administrated through tail vein at a volume of 2 ml/kg 2 wk after lentiviral injection and 7 days after intraperitoneal implantation of micro-osmotic pumps (29). Rats with the implantation of 2 micro-osmotic pumps were randomly divided into four groups *1*) N.S. (normal saline) control ($n = 6$); *2*) G/L (GalN/LPS) ($n = 10$); *3*) G/L + LV-shRNA-NC ($n = 10$); and *4*) G/L + LV-shRNA-PKC-α ($n = 10$). After administration of saline and GalN/LPS, all rats were housed individually in metabolic cages. Blood was sampled through the saphenous vein 12 h after exposure to GalN/LPS for GFR measurement. Liver and renal specimens were fixed with 4% paraformaldehyde solution for histopathologic examination. Frozen specimens were used for quantitative analysis of PKC-α and IP_3R1 by Western blot and real-time RT-PCR analyses. Portions of renal tissues were collected for isolation of glomeruli for the determination of intracellular calcium content and glomerular inulin space (GIS).

Measurement of FITC-inulin in plasma. Because pH significantly affects FITC fluorescent intensity, all plasma samples were buffered to pH 7.4 with 500 mM HEPES (18). Fluorescent intensity was determined using Thermo Scientific Varioskan Flash with excitation at 485 nm and emission at 538 nm.

A standard curve for blood samples was generated using FITC-inulin concentrations of 0–2.5 μg/ml. The linear correlation between fluorescent intensity and inulin concentration was established by measuring fluorescent intensity in serial dilutions of an FITC-inulin solution of known concentration. A regression coefficient of 0.99 was achieved between fluorescent readings and plasma FITC-inulin concentration, confirming the reliability of Thermo Scientific Varioskan Flash to measure FITC-inulin.

Calculation of GFR. GFR was evaluated 12 h after GalN/LPS exposure and 7 days after implantation of micro-osmotic pumps based on the inulin clearance equation (inulin clearance = inulin infusion rate/steady-state blood inulin concentration), as we described previously (29). GFR_1 was expressed in microliters per minute (ml/min), and GFR_2 was corrected further by kilogram body

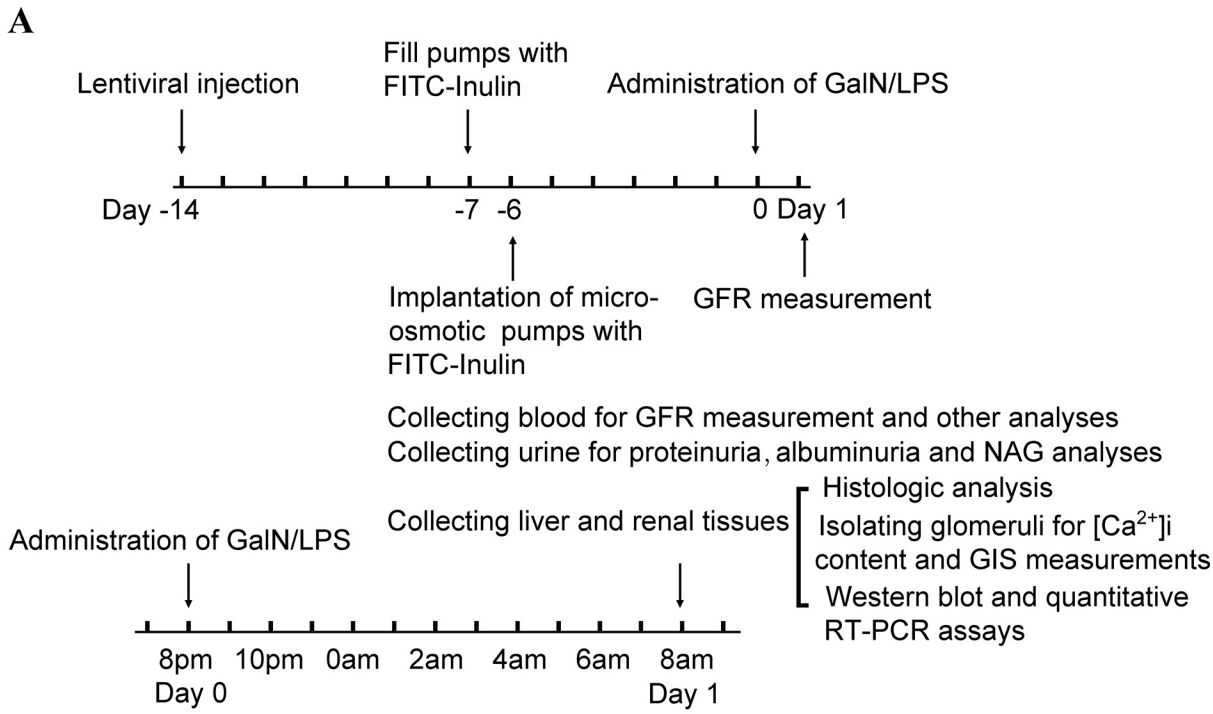

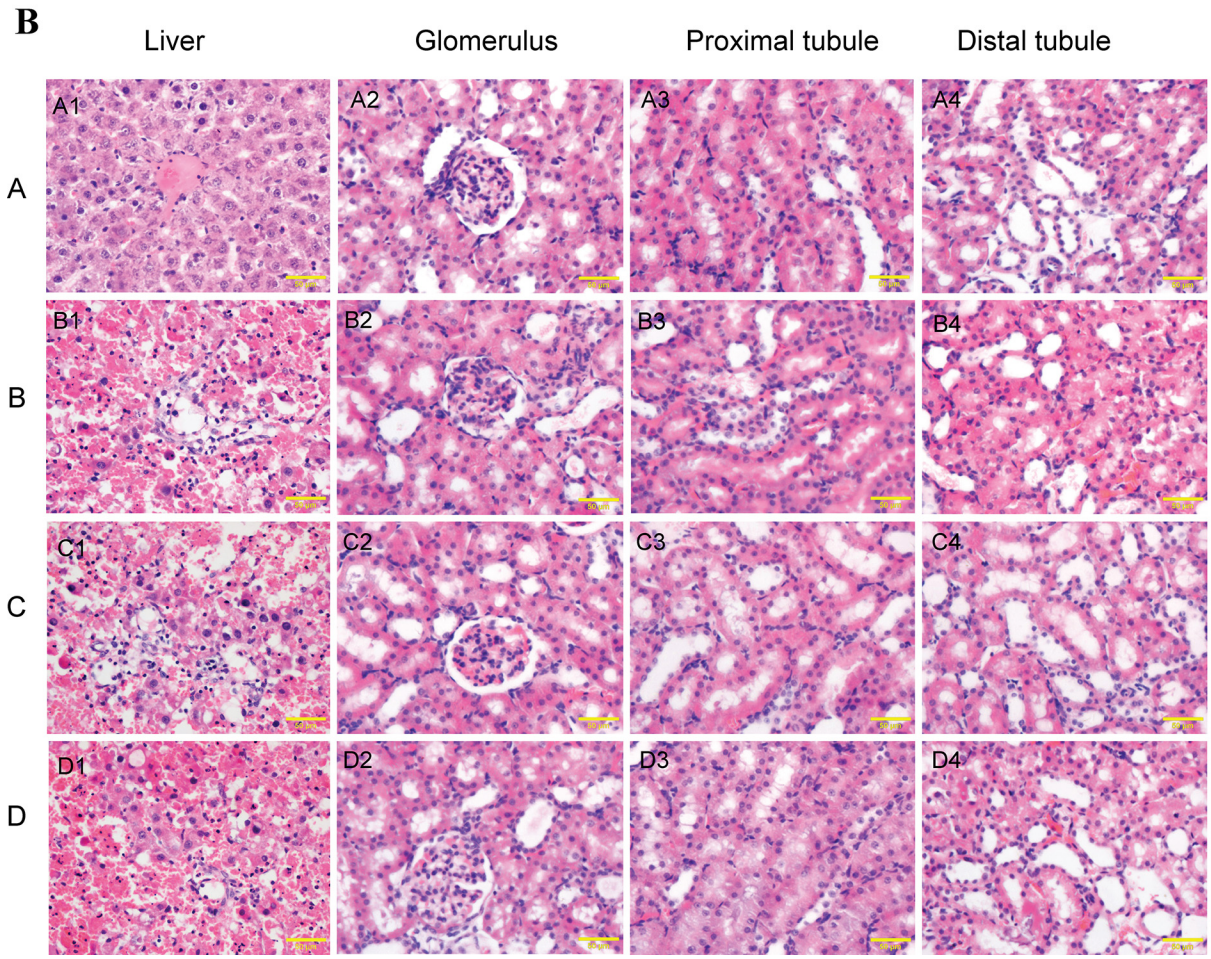

weight (ml·min^{-1}·kg body wt^{-1}). GFR_3 was calculated in microliters per minute per gram kidney weight (ml·min^{-1}·g kidney wt^{-1}). GFR_2 and GFR_3 reflect the GFR more precisely than GFR_1 due to a further correction by body and kidney weight (29).

Isolation of glomeruli from rats exposed to GalN/LPS. Glomeruli were isolated by a gradual sieving technique. Briefly, the renal capsule was removed and the cortex was minced with a razor blade to a paste-like consistency and strained through a 250-μm steel sieve. The suspension was further filtered through two consecutive steel sieves (120 and 70 μm). The glomeruli that were retained at the top of a 70-μm sieve were washed and resuspended in ice-cold PBS. Tubular contamination was <5%, as assessed under a light microscope. The entire procedure was performed in an ice bath within 1 h (26, 28). Isolated glomeruli were used for $[Ca^{2+}]_i$ and GIS measurements.

$[Ca^{2+}]_i$ measurement in glomeruli. A total of 4,000 glomeruli were suspended in 400 μl of Hank's saline solution (containing 1% bovine serum albumin). Glomeruli were incubated with fura-2-AM (10 μM; Dojindo, Tokyo, Japan) at 37°C in a shaking water bath in dark for 45 min. Fluorescent excitation of fura-2 was performed at 340/380 nm, and emission was detected above 510 nm. After the base line was recorded, the ratio of fluorescent intensity (340/380 nm) for each sample was recorded under treatment with ET-1 (100 nM; Sigma). Cytosolic $[Ca^{2+}]_i$ in glomeruli was measured during a 0.1 s exposure at 20.0-s intervals for 10 min using Thermo Scientific Varioskan Flash. At the end of each experiment, $CaCl_2$ (2.5×10^{-3} M) and EGTA (5 mM) were added to obtain maximal fluorescent intensity (F_{max}) and minimal fluorescence (F_{min}), respectively. The calculation equation of calcium concentration was as follows (7, 27): $[Ca^{2+}]_i$ (nmol/l) $= K_d \times [(R - R_{min})/(R_{max} - R)] \times (F_0/F_s)$. Here K_d equals 224 nmol/l.

Determination of GIS. Approximately 4,000 glomeruli were suspended in 400 μl of ice-cold Ca^{2+}-free buffer solution containing 1% bovine serum albumin, incubated with FITC-inulin (100 μg) at 37°C in a shaking water bath for 30 min and then equally divided into two parts. Half of the glomeruli were treated with ET-1 (100 nM) for 10 min, and the rest of the glomeruli were used as a control. After ET-1 treatment, glomeruli were centrifuged at 5,000 *g* for 5 s. Twenty microliters of supernatant and whole glomerular pellets were separately suspended in 500 μl of 0.3% Triton X-100 solution overnight. Fluorescent intensity (FI) of glomeruli was measured with Thermo Scientific Varioskan Flash. GIS of a single glomerulus was calculated as follows (26, 28):

$$\mathrm{GIS}(\mathrm{nl/glomerulus}) = \frac{\mathrm{FI-pellet}(\mu\mathrm{g/ml})}{\mathrm{FI-supernatant}(\mu\mathrm{g/ml})} \times \frac{1}{\text{number of glomeruli in pellet}}.$$

Serum biochemical analysis. Serum levels of alanine aminotransferase (ALT), aspartate aminotransferase (AST), creatinine (Cr), blood urea nitrogen (BUN), potassium (K^+), sodium ion (Na^+), chloride ion (Cl^-), TNF-α, and ET-1 were determined using commercial kits. Serum levels of TNF-α and ET-1 were quantified by ELISA using commercial kits (R&D Systems, Abingdon, UK).

Proteinuria, albuminuria, and urine N-acetyl-β-D-glucosaminidase analysis. The urine samples were collected over 12 h from rats placed in metabolic cages. Protein concentration was measured using a modified Lowry assay. Urine levels of albuminuria and *N*-acetyl-β-D-glucosaminidase (NAG) were performed by ELISA as instructed by the manufacturers and used to be indicators of renal tubular injury.

Histologic analysis. Liver and kidney specimens were fixed in 10% formalin and embedded in paraffin for histopathological analysis.

Electronic microscopy specimen preparation and examination. The electronic microscopy preparation of renal cortex specimens was performed as described previously (15), and the sections were observed in JEOL JEM 1230 Transmission Electron Microscope (29).

Cell culture and transfection. A GMC line (CRL-2573) was obtained from American Type Culture Collection (Manassas, VA). GMC cells were cultured at 37°C in a 5% CO_2 humidified incubator with high-glucose DMEM medium containing 10% FBS, 100 U/l penicillin, and 100 mg/l streptomycin (12).

Cells were plated in six-well plates (35 mm) and grown to 60–80% confluence at the time of transfection. Before transfection, RNAi duplex-Lipofectamine RNAiMAX complexes were prepared following the manufacturer's protocol based on preliminary results. Cells were cultured with Lipofectamine RNAiMAX reagent plus siRNA at a ratio of 6 μl:6 μl (120 pmol), respectively. After 6 h, 2 ml of fresh complete DMEM medium were changed and cells were cultured for 24 h. Cells were divided into four groups *1*) siRNA-NC; *2*) siRNA-NC + TNF-α; *3*) siRNA-PKC-α; and *4*) siRNA-PKC-α + TNF-α. TNF-α (100 ng/ml) was added 24 h before cells were collected.

Treatments of GMCs with TNF-α. GMCs were stimulated with TNF-α (100 ng/ml) for 2 to 24 h before being harvested for RNA or protein extraction (30).

$[Ca^{2+}]_i$ measurement in transfected GMCs. GMCs transfected with siRNA against PKC-α were treated with TNF-α (100 ng/ml) for 24 h, then digested with 0.25% trypsin, and suspended in complete DMEM medium. Cytosolic $[Ca^{2+}]_i$ in GMCs was measured during a 0.1-s exposure at 6.0-s intervals for 3 min using Thermo Scientific Varioskan Flash. Other process and formula were the same as $[Ca^{2+}]_i$ measurement in glomeruli (7, 27).

Real-time quantitative RT-PCR. Total RNA was isolated from the scaffold using a Trizol (Takara)-based protocol. The concentration and purity of mRNA were determined by spectrophotometry at 260 and 280 nm and diluted to 500 ng/μl with DEPC-treated water. RNA was incubated at 37°C for 15 min, followed by 85°C for 5 s for reverse transcription to generate cDNA. The cDNA underwent 40 cycles of PCR (95°C for 30 s, 95°C for 5 s, and 60°C for 30 s) in TP800 Thermal Cycler Dice Real Time System (Takara). Primer sequences of rat IP_3R1 were 5′-TCTGGCCAGCTGTCAGAACTAAAG-3′ (forward) and 5′-GTGGGTTGACATTCATGTGAGGA-3′ (reverse). Primer sequences of rat PKC-α were 5′-TCCAGGATGACGACGTGGAG-3′ (forward) and 5′-CGTTGACGTATTCCATGACGAAG-3′ (reverse). Primer sequences of rat GAPDH were 5′-GACAACTTTGGCATCGTGGA-3′ (forward) and 5′-GACAACTTTGGCATCGTGGA-3′ (reverse). Relative levels of *IP_3R1* and *PKC-α* gene expression were calculated based on amplification of a standard curve after a series of cDNA dilutions. GAPDH was used as a housekeeping control. Each sample was assayed in triplicate (29).

Western blot analysis of IP_3R1. To detect PKC-α, SP-1, JNK/p-JNK, and IP_3R1 proteins, cells were treated and washed with ice-cold

Fig. 1. Timeline of animal experimental design and normal renal morphology during acute liver injury. *A*: timeline of animal experimental design and procedures performed in rats. GalN, D-galactosamine hydrochloride; GFR: glomerular filtration rate; GIS: glomerular inulin space; NAG, *N*-acetyl-β-D-glucosaminidase; FITC, fluorescein isothiocyanate. *B*: liver and renal morphology of fulminant hepatic failure. *A1–A4*: normal saline (N.S.) controls. *B1–B4*: GalN/LPS (G/L) group. *C1–C4*: G/L + LV-shRNA-NC group. *D1–D4*: G/L + LV-shRNA-PKC-α group. Morphology of GalN/LPS-induced acute liver injury in all groups. Liver histology from rats 12 h after treatment with GalN/LPS shows massive hemorrhage and necrosis. Extensive necrosis is accompanied with fracture of hepatocellular cords, loss of lobular structure, sinusoid expansion, and Kupffer cell proliferation. Damaged hepatocytes appear to have their nuclei dissolved with nuclear debris or pycnosis. Severe liver necrosis is accompanied by biliary ductular reaction (*B*, *C1*) and sinusoidal congestion (*B*, *B1*, *C1*, and *D1*) as seen 12 h after GalN/LPS challenge. No changes in liver morphology were observed between G/L + LV-shRNA-NC group and G/L + LV-shRNA-PKC-α group. None of the GalN/LPS-exposed rats had obvious morphologic alterations in the glomerulus or proximal and distal tubule of rats with GalN/LPS exposure. Hematoxylin and eosin staining is shown with magnification at ×400.

PBS. Total cell protein was extracted in RIPA lysis buffer (Beyotime, Shanghai, China) and total renal tissue protein was extracted using T-PER Tissue Protein Extraction (Thermo, Rockford, UIL), followed by centrifugation (12,000 *g*, 12 min). Protein concentration was determined with a BCA protein assay reagent kit (Pierce Biotechnology, Thermo). Equal amounts of protein were applied to 7% (for IP_3R1) or 10% (for SP-1 and PKC-α) SDS-PAGE and electrophoresed. Proteins were transferred onto a PVDF membrane (Millipore), which was blocked with 5% fat-free milk for 2 h. After blocking, the PVDF membrane was immunoblotted with a primary antibody (polyclonal IP_3R1 antibody, polyclonal PKC-α antibody, SP-1 antibody, or JNK/p-JNK antibody) overnight. The membrane was washed three times with a Tris·HCl-NaCl-Tween 20 solution to remove unbound antibody. The membrane was then incubated with horseradish peroxidase-conjugated goat-anti-rabbit IgG for 1 h at room temperature. The membrane was washed three times with Tris·HCl-NaCl-Tween 20 to remove unbound secondary antibody and developed with a Luminol chemiluminescent detection kit (Pierce Biotechnology, Thermo). Protein expression was quantified by densitometry. β-Actin and GAPDH were used internal loading controls. Relative protein levels were calculated based on a densitometric count ratio of IP_3R1 over β-actin bands (29).

Chromatin immunoprecipitation. Chromatin immunoprecipitation (ChIP) assays were performed as described by Svoteliset et al. (25). Cells were transfected with siRNA against *PKC-α* or control siRNA using Lipofectamine RNAiMAX, and the culture medium was replaced with fresh complete DMEM 6 h after transfection. Cells were cross linked in medium containing 1% formaldehyde for 10 min at 37°C before the reaction was stopped with glycine 24 h after transfection. Cells were resuspended in SDS lysis buffer (1% SDS, 10 mM EDTA, and 50 mM Tris·HCl, pH 8.1) with 1× protease inhibitor cocktail (Roche Molecular Biochemicals, Indianapolis, IN) and sonicated with a Handy Sonic (model UR-20P) for six cycles of 10 s at 60% attitude followed by centrifugation at 14,000 *g* in 4°C for 10 min to obtain DNA fragments between 200 and 500 bp. Supernatants were collected and diluted in ChIP dilution buffer (0.01% SDS, 1.1% Triton, 1.2 mM EDTA, and 167 mM Tris·HCl, pH 8.1) followed by immunoclearing with protein A agarose/salmon sperm DNA (Millipore) for 30 min at 4°C. ChIP preparations were incubated overnight at 4°C with specific antibodies. Protein A agarose/salmon sperm DNA

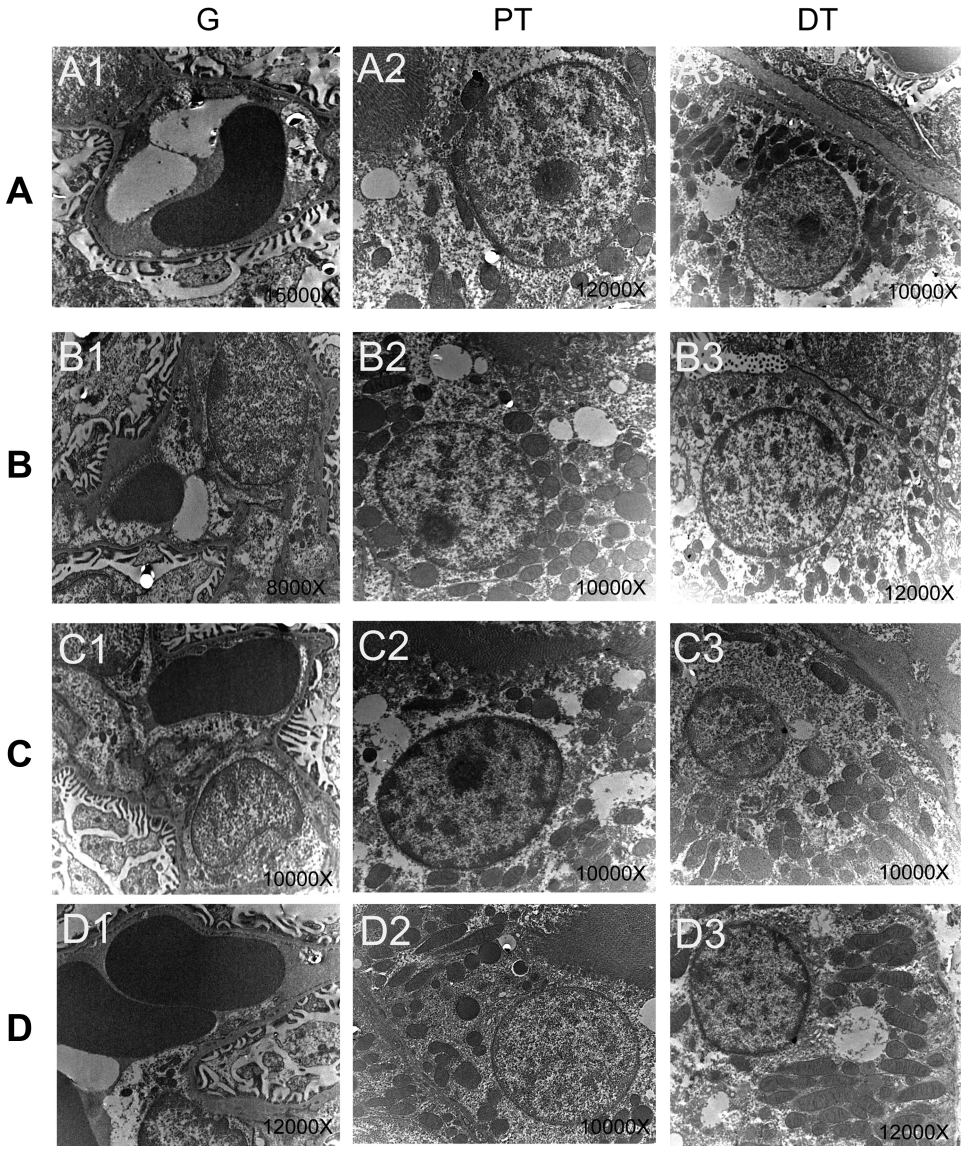

Fig. 2. Renal electronic microscopic images in GalN/LPS-induced acute liver failure. Renal ultrastructure of GalN/LPS-induced acute liver failure was examined under electron microscope. *A*: N.S. controls. *B*: GalN/LPS group. *C*: G/L + LV-shRNA-NC group. *D*: G/L + LV-shRNA-PKC-α group. No significant abnormalities were found in the glomerulus (G: *A1–D1*), proximal tubule (PT; *A2–D2*), and distal tubule (DT; *A3–D3*) of rats with GalN/LPS exposure or in rats treated with G/L + LV-shRNA-NC or G/L + LV-shRNA-PKC-α.

Table 1. *Serum levels of ALT, Cr, BUN, K^+, Cl^-, Na^+, and cytokines*

Group	N.S. ($n = 6$)	G/L ($n = 5$)	G/L + LV-shRNA-NC ($n = 4$)	G/L + LV-shRNA-PKC-α ($n = 5$)
ALT, IU/l	51.8 ± 11.3	3,191.0 ± 1,107.8^{aa}	2,740.0 ± 1,202.5^{aa}	3,348.0 ± 1,322.5^{aa}
AST, IU/l	34.3 ± 2.2	6,574.5 ± 3,912.7^{aa}	7,402.5 ± 4,782.7^{aa}	6,323.0 ± 4,658.8^{a}
Cr, μmol/l	43.6 ± 15.0	68.3 ± 4.7^{aa}	63.9 ± 5.5^{a}	45.1 ± 7.7^{b}
BUN, mmol/l	5.0 ± 1.1	15.8 ± 8^{aa,b}	12.5 ± 3.0^{aa}	7.9 ± 2.1^{a,b}
K^+, mmol/l	5.7 ± 0.7	5.8 ± 0.5	6.1 ± 0.85	6.3 ± 1.0
Cl^{-1}, mmol/l	94.1 ± 4.7	90.5 ± 2.3	94.8 ± 3.0	99.7 ± 5.0^{a}
Na^+, mmol/l	135.3 ± 3.5	137.7 ± 4.9	132.8 ± 3.1	140.5 ± 2.8^{a,b}
TNF-α, ng/l	77.32 ± 24.02	541.99 ± 28.17^{aa}	546.31 ± 17.51^{aa}	552.90 ± 19.83^{aa}
ET-1, μg/l	50.21 ± 11.48	281.32 ± 9.34^{aa}	263.67 ± 18.77^{aa}	269.68 ± 12.98^{aa}
GFR_1, ml/min	2.29 ± 0.22	0.70 ± 0.12^{aa}	0.84 ± 0.07^{aa}	1.26 ± 0.23^{aa,b}
GFR_2, ml·min^{-1}·kg body wt^{-1}	11.24 ± 4.18	4.16 ± 1.31^{aa}	5.23 ± 0.80^{aa}	7.40 ± 1.17^{a,b}
GFR_3, ml·min^{-1}·kg kidney wt^{-1}	1.30 ± 0.36	0.40 ± 0.13^{aa}	0.52 ± 0.10^{aa}	0.80 ± 0.17^{aa,b}

Data represent means ± SE. BUN, blood urea nitrogen; N.S., normal saline; G/L, D-galactosamine hydrochloride (GalN)/LPS; ET-1, endothelin-1; GFR, glomerular filtration rate. $^{a}P < 0.05$, as compared with N.S. control group. $^{aa}P < 0.01$, compared with N.S. control group. $^{b}P < 0.05$, compared with G/L + LV-shRNA-NC group. $^{bb}P < 0.01$, compared with G/L + LV-shRNA-NC group.

was added and washed sequentially with low-salt buffer, high-salt buffer, LiCl buffer, and 1× TE buffer. Protein-DNA complexes were eluted, and crosslinking was reversed at 65°C overnight. DNA fragments were purified by phenol/chloroform and absolute ethyl alcohol and analyzed by PCR. Primer sequences for the IP_3R1 promoter region were 5′-TTCCGGGCCTATATAAGCGG-3′ (forward) and 5′-GTTAGGATGGGAGCGGAACA-3′ (reverse). Immunoprecipitated DNA was amplified by PCR for 45 cycles (95°C for 15 s, 57°C for 15 s, and 72°C for 20 s) with the touchdown amplification protocol used for chemokine expression analysis.

Statistical analysis. All results presented are representative of at least three separate experiments and are expressed as means ± SE. SPSS version 17.0 software was used for statistical analysis and compared using one-factor ANOVA and least significant difference for multiple comparisons between groups. $P < 0.05$ was considered statistically significant.

RESULTS

Renal failure model induced by GalN/LPS treatment. Liver tissues stained with hematoxylin and eosin presented histologically extensive hepatic necrosis and severe hemorrhage in part of lobules. Extensive necrosis is accompanied with fracture of hepatocellular cord, loss of lobular structure, sinusoid expansion, and Kupffer cell proliferation. Damaged hepatocytes appear to have their nuclei dissolved with nuclear debris or pycnosis. Severe liver necrosis is accompanied by biliary ductular reaction (Fig. 1*B*, *C1*) and sinusoidal congestion (Fig. 1*B*, *B1*, *C1*, and *D1*) as seen 12 h after GalN/LPS challenge. None of the GalN/LPS-exposed rats had obvious renal morphologic alterations in histological examination (Fig. 1*B*). Micrographs of electronic microscopy did not show any abnormalities in renal cortex in all groups (Fig. 2). Representing marked renal dysfunction without structural or histologic alteration in severe hepatic damage is the characteristics of acute renal insufficiency and is a valuable model for testing molecular intervention with an RNAi approach.

Effect of silencing PKC-α in animals with FHF. G/L group mortality reached 40% (4/10) 12 h after the administration of GalN/LPS, 39% (9/13) in G/L + LV-shRNA-NC group, and 32% (8/25) in G/L + LV-shRNA-PKC-α group. GalN/LPS treatment led to a marked increase in serum ALT (up to 65-fold), AST (up to 216-fold), Cr (1.6-fold), BUN (up to 3.2-fold), TNF-α (up to 7.2-fold), and ET-1 (up to 5.6-fold) levels (Table 1). Preadministration of lentivirus harboring shRNA against PKC-α attenuated renal failure in FHF rats as indicated by improved BUN (down by 50%) and Cr (down by 33.7%) in the G/L+LV-shRNA-PKC-α group in comparison with the G/L and G/L + LV-shRNA-NC groups (Table 1) and partially improved rat mortality from nearly 40 to 32%.

Suppressing PKC-α expression increased GFR in rats with FHF. FITC-inulin clearance was measured under a steady-state condition to reflect GFR. After implantation of microosmotic pumps in the peritoneal cavity, rats experienced a significant weight loss over a few days and then gradually recovered to preoperative body weight by *day 7*. Thus inulin clearance was determined 7 days after implantation of microosmotic pumps and 12 h after GalN/LPS exposure. GFR was calculated from plasma inulin levels and a known pump infusion rate. GalN/LPS intoxication decreased GFR_1 in the G/L and G/L + LV-shRNA-NC groups by 31 and 37% of the N.S. controls, respectively. GFR_1 values in the G/L + LV-shRNA-PKC-α group were significantly restored compared with the G/L and G/L + LV-shRNA-NC groups (80 and 50%). GFR values are presented in Table 1 after correction with body weight (per kilogram, GFR_2) and kidney weight (per gram, GFR_3). These data confirmed renal malfunction during FHF caused by GalN/LPS intoxication and prevention of renal insufficiency by PKC-α shRNA lentiviral administration.

Proteinuria, albuminuria, and urine NAG in FHF rats. GalN/LPS treatment did NOT cause a marked increase in proteinuria, albuminuria, and urine NAG levels in FHF rats. There is no significant difference in NAG (one of the urinary tubular injury biomarkers) levels between controls and GalN/LPS-exposed rats and those receiving PKC-α shRNA lentiviral administration (Table 2).

Effects of PKC-α inhibition on PKC-α and IP_3R1 expression in renal tissue. Quantitative RT-PCR was performed to determine PKC-α and IP_3R1 mRNA expression in renal tissue.

Table 2. *Levels of proteinuria, albuminuria, and urine NAG*

Group	N.S. ($n = 10$)	G/L ($n = 6$)	G/L +LV-shRNA-NC ($n = 5$)	G/L +LV-shRNA-PKC-α ($n = 5$)
Proteinuria, mg/dl	46.7 ± 19.01	41.5 ± 27.5	47.2 ± 17.8	44.8 ± 25.2
Albuminuria, μg/dl	2.44 ± 0.84	2.19 ± 2.21	2.14 ± 0.98	2.11 ± 2.88
NAG, mUI/ml	31.5 ± 5.87	29.7 ± 4.67	27.4 ± 5.03	31.2 ± 9.52

Data represent means ± SE. NAG, *N*-acetyl-β-D-glucosaminidase.

PKC-α (1 vs. 3.45, $P < 0.01$ and 1 vs. 3.27, $P < 0.01$) and IP_3R1 (1 vs. 2.91, $P < 0.01$ and 1 vs. 3.20, $P < 0.01$) mRNA levels in the G/L group and G/L + LV-shRNA-NC groups were gradually increased after GalN/LPS exposure compared with N.S. controls. Compared with the G/L + LV-shRNA-NC group, PKC-α (3.45 vs. 0.69, $P < 0.01$) and IP_3R1 (2.91 vs. 3.20, $P < 0.01$) mRNA levels in the G/L + LV-shRNA-PKC-α group were markedly decreased (Fig. 3, *A* and *B*). PKC-α (1 vs. 2.78, $P < 0.05$ and 1 vs. 2.80, $P < 0.05$) and IP_3R1 (1 vs. 1.94, $P < 0.01$ and 1 vs. 1.75, $P < 0.01$) protein levels were increased in the G/L and G/L + LV-shRNA-NC groups at 12 h compared with N.S. controls. Compared with the G/L + LV-shRNA-NC group, PKC-α and IP_3R1 protein levels in the G/L + LV-shRNA-PKC-α group were markedly decreased (2.78 vs. 1.14, $P < 0.01$ for PKC-α; 1.94 vs. 0.55 for IP_3R1) (Fig. 3, *C* and *D*). These findings suggest that *IP_3R1* and *PKC-α* gene expression in kidneys was affected during FHF and may be responsible for the renal insufficiency.

Effects of silencing PKC-α on glomerular $[Ca^{2+}]_i$ and GIS. GalN/LPS exposure increased glomerular cytosolic $[Ca^{2+}]_i$ levels in the G/L (1 vs. 2.22 $P < 0.01$) and G/L + LV-shRNA-NC groups (1 vs. 2.14, $P < 0.01$) compared with N.S. controls, and $[Ca^{2+}]_i$ levels were not different between the G/L + LV-shRNA-NC group and the G/L group. Preadministration of LV-shRNA-PKC-α markedly reduced $[Ca^{2+}]_i$ levels compared with the G/L + LV-shRNA-NC group (2.22 vs. 1.24, $P < 0.01$) (Fig. 3*E*). Changes in GIS reflect glomerular size and indirectly indicate vascular dilation/constriction sta-

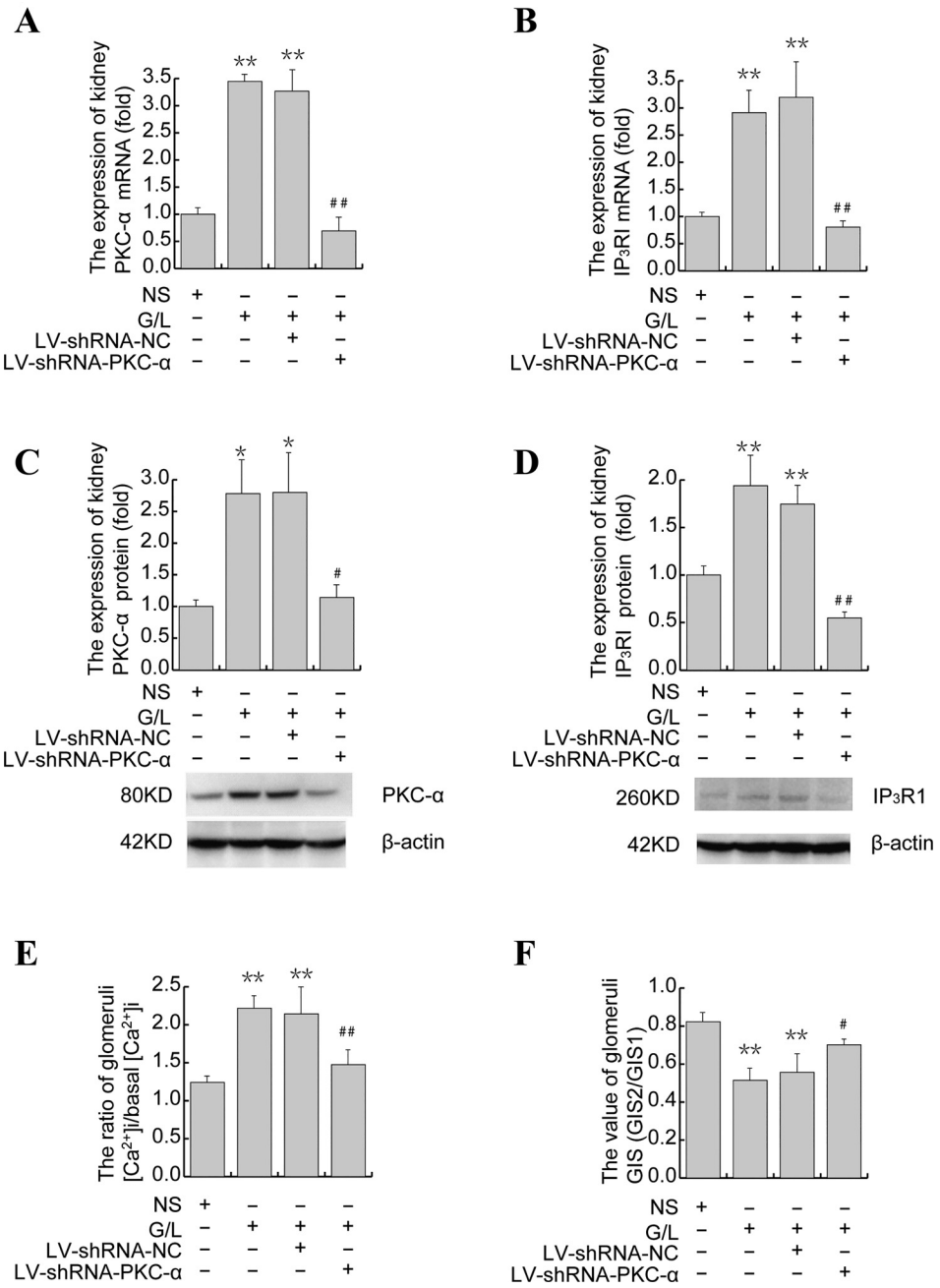

Fig. 3. Effects of silencing PKC-α on PKC-α mRNA protein levels, type 1 inositol 1,4,5-trisphosphate receptor (IP_3R1) mRNA levels, GIS, and glomerular calcium content in renal tissues. *A*: changes in PKC-α mRNA levels after exposure to GalN/LPS. *B*: changes in IP_3R1 mRNA levels after exposure to GalN/LPS. *C*: changes in PKC-α protein levels after exposure to GalN/LPS. *D*: changes in IP_3R1 protein level after GalN/LPS treatment. *E*: ratio of basal over sustained cytosolic Ca^{2+} concentration ($[Ca^{2+}]_i$) was used to show the changes in calcium levels after exposure to GalN/LPS and PKC-α silencing. *F*: the GIS ratio was determined in isolated glomeruli in the presence of FITC-inulin. GIS2 represents the ratio after endothelin-1 (ET-1) treatment; GIS1 was used a control. Data represent the means ± SE ($n = 3$). *$P < 0.05$, compared with saline controls. **$P < 0.01$, compared with saline controls. #$P < 0.05$, compared with GalN/LPS group. ##$P < 0.01$, compared with G/L + LV-shRNA-NC group.

tus. Ratios of GIS_2 (treated with ET-1) over GIS_1 (control) are shown in Fig. 3*F*. The GIS ratios in the G/L (1 vs. 0.51, $P < 0.01$) and G/L + LV-shRNA-NC (1 vs. 0.56, $P < 0.01$) groups were markedly decreased compared with the N.S. controls. The ratios were not statistically different between the G/L + LV-shRNA-NC group and the G/L group. The GIS ratio in the G/L + LV-shRNA-PKC-α group was restored compared with the G/L + LV-shRNA-NC group (0.56 vs. 0.70, $P < 0.01$), indicating that PKC-α plays a critical role in modulating renal vascular constriction. We observed that AKI and decrease of GFR in FHF rats caused by GalN/LPS exposure were accompanied with upregulated IP_3R1 expression and increasing glomerular calcium content. The PKC-α silencing in FHF rats improved these abnormalities. However, the molecular mechanisms of how PKC-α silencing attenuated the extent of AKI in FHF are not fully understand. Therefore, we employed GMCs to further investigate the effects on TNF-α on PKC-α and IP_3R1.

TNF-α-stimulated PKC-α and IP_3R1 expression in GMCs. We further investigated the molecular mechanism of TNF-α on PKC-α and IP_3R1 expression in GMCs. Quantitative analysis demonstrated that PKC-α mRNA started to increase at 4 h and reached higher levels at 8 h after TNF-α treatment ($P < 0.05$), which were sustained till 24 h (Fig. 4*A*). The expression levels of PKC-α protein expression started to increase at 4 h, reached the highest at 8 h ($P < 0.05$), and returned to nearly a basal level by 24 h (Fig. 4*B*). A significant induction of IP_3R1 mRNA occurred by 2 h after TNF-α treatment, reached a maximum at 8 h ($P < 0.01$) compared with basal levels, and returned to a basal level at 24 h (Fig. 4*C*). Compared with the basal level, IP_3R1 protein levels started to increase at 4 h after TNF-α treatment, increased to the highest levels at 8 h, and were sustained for 24 h ($P < 0.05$) (Fig. 4*D*). We observed an increase in mRNA levels before an increase in protein levels. The increase in IP_3R1 mRNA levels by TNF-α stimulation could be partly due to an effect on transcription of IP_3R1 gene. The increased expression of IP_3R1 may be partly due to increased synthesis of the PKC-α.

The effect of silencing PKC-α on TNF-α-stimulated IP_3R1 expression and the change of cytosolic $[Ca^{2+}]_i$ after ET stimulation in GMCs. PKC-α mRNA expression in GMC cells transfected with siRNA was determined by real-time RT-PCR 8 h after TNF-α treatment. Western blot analysis was performed to determine IP_3R1 and PKC-α protein levels 24 h after

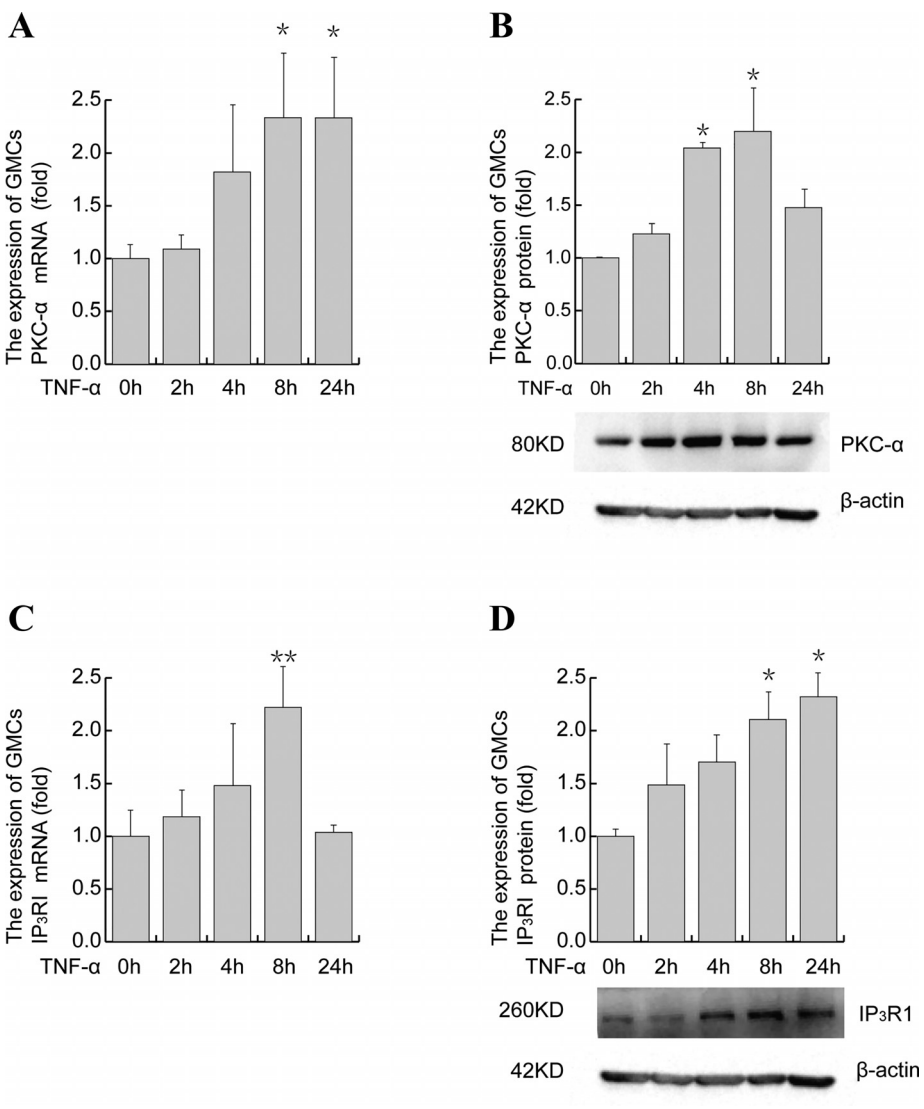

Fig. 4. Effects of TNF-α stimulation on PKC-α and IP_3R1 mRNA and protein expression. *A*: quantitative results of PKC-α/GAPDH mRNA ratios using controls as a reference. *B*: representative Western blots for PKC-α protein and quantitative results of PKC-α/β-actin. *C*: quantitative results of IP_3R1/GAPDH mRNA ratios using controls as a reference by a quantitative RT-PCR assay. *D*: representative Western blots for IP_3R1 protein and quantitative results of IP_3R1/β-actin densitometry. Data represent the means ± SE ($n = 3$). *$P < 0.05$, compared with 0 h. **$P < 0.01$, compared with 0 h.

TNF-α treatment. Compared with the siRNA-NC group, PKC-α mRNA (2.69-fold) and protein (2.45-fold) expression was significantly increased ($P < 0.01$) by TNF-α treatment (Fig. 5, *A* and *C*). There was a marked decrease in PKC-α mRNA and protein expression levels after *PKC-α* silencing ($P < 0.01$). TNF-α treatment resulted in enhanced IP_3R1 expression at both the mRNA (2.53-fold) and protein (2.85-fold) levels in the siRNA-NC + TNF-α group compared with the siRNA-NC group ($P < 0.01$) (Fig. 5, *B* and *D*). Compared with TNF-α stimulation alone, silencing *PKC-α* suppressed TNF-α-induced expression of IP_3R1 at the mRNA and protein levels ($P < 0.01$) (Fig. 5, *B* and *D*). ET-1 is a potent vasoconstrictor of the renal vascular bed. The ratio of cytosolic $[Ca^{2+}]_i$ in GMCs treated with ET-1 over basal $[Ca^{2+}]_i$ is shown in Fig. 5*E*. Using the Ca^{2+}-sensitive dye fura-2-AM, we were able to show that ET-1 triggered a marked increase in the $[Ca^{2+}]_i$ ratio in GMC cells in the first, second and third minute in the siRNA-NC + TNF-α group ($P < 0.05$). Silencing *PKC-α* completely abrogated ET-1-elicited release of restored $[Ca^{2+}]_i$ in both siRNA-PKC-α and siRNA-PKC-α + TNF-α groups ($P < 0.01$).

TNF-α regulates SP-1 expression and its binding to the IP₃R1 promoter. SP-1 protein expression was obviously increased 2–24 h after TNF-α treatment and reached peak levels at 8 h ($P < 0.01$) (Fig. 6*A*). GMCs were treated with TNF-α for 4–24 h, and the ChIP assay was performed with SP-1 antibody and primers specific to the SP-1 binding site in the IP_3R1 promoter region. The findings demonstrated that TNF-α treat-

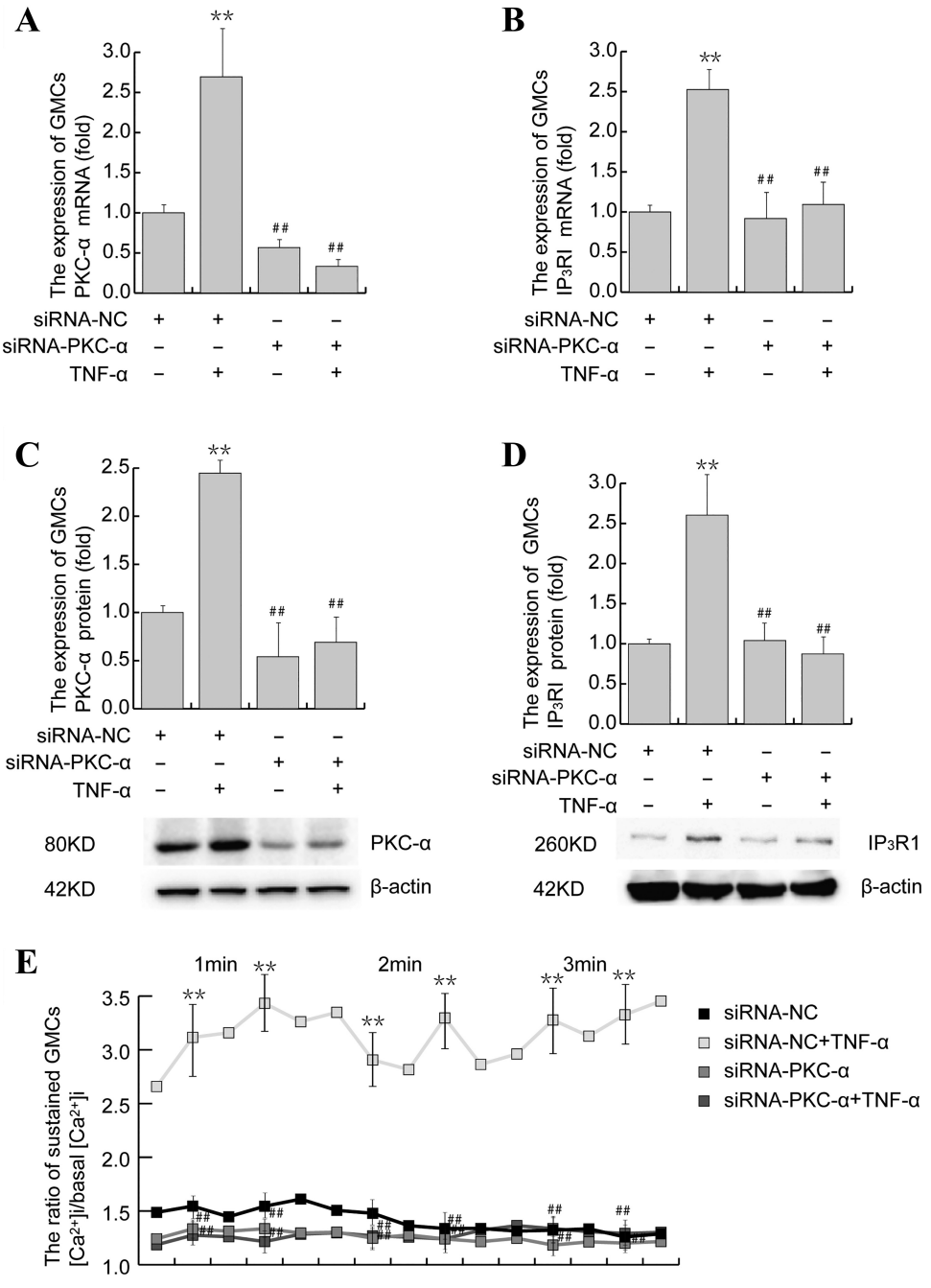

Fig. 5. Effects of silencing PKC-α on PKC-α and IP_3R1 mRNA and protein expression. *A*: quantitative results of PKC-α/GAPDH mRNA ratios using the controls as a reference ($n = 3$). *B*: quantitative results of IP_3R1/GAPDH mRNA ratios using the controls as a reference ($n = 3$). *C*: representative Western blots for PKC-α protein and quantitative results of PKC-α/β-actin densitometry ($n = 3$). *D*: representative Western blots for IP_3R1 protein and quantitative results of IP_3R1/β-actin densitometry ($n = 6$). *E*: ratio of sustained $[Ca^{2+}]_i$ over basal levels was used to show changes in calcium levels after TNF-α exposure and PKC-α silencing. Data represent the means ± SE ($n = 3$). $^{**}P < 0.01$, compared with siRNA-NC group. $^{\#\#}P < 0.01$, compared with siRNA-NC + TNF-α group.

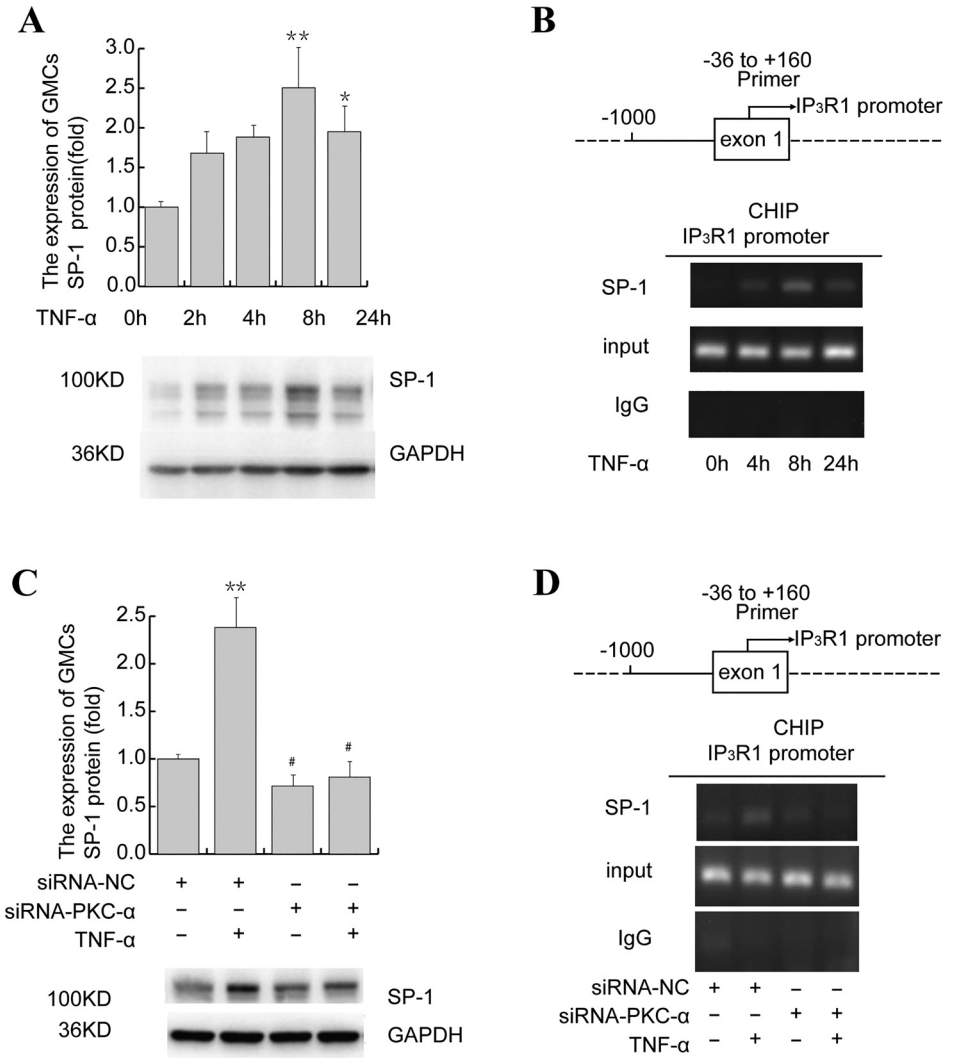

Fig. 6. Effects of PKC-α silencing on specificity protein-1 (SP-1) protein expression and chromatin immunoprecipitation-defined SP-1 binding sites. *A*: representative Western blots for SP-1 protein and quantitative results of SP-1/GAPDH densitometry. *B*: SP-1 binding to the promoter region following TNF-α stimulation. *C*: Western blot analysis of changes in SP-1 protein levels after TNF-α treatment. *D*: effects of silencing PKC-α on SP-1 binding to the promoter. Data represent the means ± SE ($n = 3$). *$P < 0.05$, compared with 0 h or siRNA-NC group. **$P < 0.01$ compared with 0 h or siRNA-NC group. #$P < 0.05$, compared with siRNA-NC + TNF-α group.

ment remarkably enhanced SP-1 binding to the IP_3R1 promoter in GMCs with a maximal effect seen at 8 h (Fig. 6*B*). TNF-α (100 ng/ml) was added 8 h before cells were collected. Compared with the siRNA-NC group, SP-1 protein expression was significantly increased ($P < 0.01$) by TNF-α treatment, and this trend was significantly mitigated by transfection with siRNA against *PKC-α* (Fig. 6*C*) ($P < 0.05$). *PKC-α* silencing also suppressed the increased binding activity of SP-1 to the IP_3R1 promoter caused by TNF-α exposure (Fig. 6*D*). Therefore, the findings confirmed that SP-1 is the transcription factor governing the IP_3R1 expression in GMCs exposed to TNF-α.

Effects of PKC-α silence on JNK/p-JNK expression. Significant induction of JNK and p-JNK protein occurred by 2 h after TNF-α treatment and reached a maximum level at 8 h ($P < 0.01$ and $P < 0.05$, respectively) compared with the basal levels. JNK and p-JNK protein levels were returned at 24 h (Fig. 7, *A* and *B*). Compared with the siRNA-NC group, JNK and p-JNK protein expression in siRNA-NC + TNF-α group was significantly increased ($P < 0.05$). It is evident from Fig. 7, *C* and *D*, that silencing PKC-α suppressed TNF-α-induced expression of JNK and the p-JNK protein in GMCs ($P < 0.05$).

Involvement JNK activation in TNF-α-induced IP_3R1 expression. GMCs were treated with a JNK inhibitor, SP600125 (10 μmol/l), for 1 h before exposure to TNF-α. The addition of SP600125 was sufficient to cause almost completely abrogated TNF-α-stimulated increase in SP-1 protein level ($P < 0.01$) (Fig. 8*A*). SP600125 suppressed TNF-α-stimulated IP_3R1 expression at both mRNA and protein levels ($P < 0.01$) (Fig. 8, *B* and *C*). These results point to a positive regulatory role of PKC-α and JNK signaling in TNF-α-induced expression of IP_3R1 in GMCs.

DISCUSSION

Fulminant or subacute hepatic failure or end-stage liver disease often accompanies AKI, and the multiple organ failure evidently increases patient mortality. There are several hypotheses regarding how AKI happens during FHF (31). A widely recognized hypothesis is when FHF occurs, the internal organs and peripheral vessels become dilated, which reduces the effective blood volume and causes overexcitation of the sympathetic nerve and renin-angiotonin systems. Endogenous vasoconstrictors, such as vasopressins (e.g., angiotonin II and norepinephrine), increase the pressure of peripheral vascular

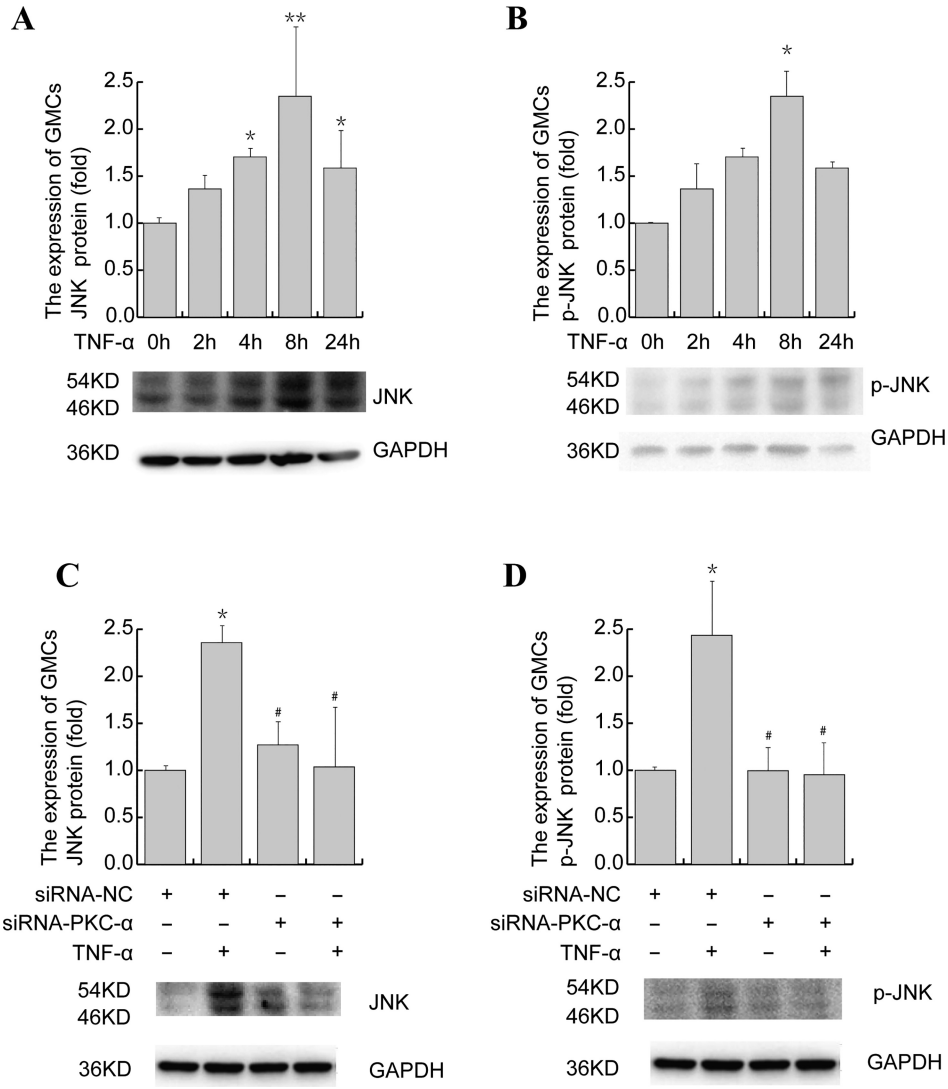

Fig. 7. Effects of TNF-α stimulation on JNK/p-JNK protein expression. *A*: Western blot analysis of changes in JNK protein levels after TNF-α exposure. *B*: Western blot analysis of changes in p-JNK protein levels after TNF-α exposure. *C*: effects of silencing PKC-α on JNK protein expression. *D*: effects of silencing PKC-α on p-JNK protein expression. Data represent the means ± SE ($n = 3$). *$P < 0.05$, compared with 0 h or siRNA-NC group. **$P < 0.01$, compared with 0 h or siRNA-NC group. #$P < 0.05$, compared with siRNA-NC + TNF-α.

beds (including the preglomerular arteriole) and arteries (renal hypoperfusion), and the consequence is uncontrolled constriction of preglomerular vessels (14). Therefore, it is conceivable that the strong constriction of renal vessels may be the dominant pathogenesis of renal failure during FHF; however, the signaling pathway underlying renal vessel constriction remains to be elucidated in an appropriate animal model.

TNF-α is an important cytokine in the development of renal disease and severe hepatopathy, and TNF-α levels are positively correlated with the severity of renal diseases (5). Administration of TNF-α antibody attenuated the renal insufficiency in FHF rats (29). These clinical or laboratory studies suggest that TNF-α plays an indispensable role in the development of AKI during FHF and may be a key factor that is directly or indirectly responsible for a reduction of GFR as shown in Table 1. IP_3R1 is an important Ca^{2+} release channel present primarily in renal GMCs and VSMCs (11). Many factors, such as TNF-α, trigger IP_3R1 expression, and in turn cause subsequent Ca^{2+} imbalance and increased cell contraction sensitivity during the progression of renal failure (4, 33). In clinical observations, serum levels of TNF-α, ET-1, and other vasoconstrictors are significantly elevated during the development of FHF, and ET-1 elicits IP_3 production as a potent vasoconstrictor of the renal vascular bed (6, 21, 23 32). The elevation of IP_3R expression in GMCs and VSMCs as observed in the present study provides more binding sites for the IP_3 ligand, promotes IP_3-mediated Ca^{2+} mobilization, and increases cell susceptibility to vasoconstrictor (e.g., ET-1). Cytosolic Ca^{2+} reserved in the endoplasmic reticulum is released into the cytoplasm, and this triggers contraction of GMCs and VSMCs, reduces glomerular filtration area, and decreases renal blood flow, thereby further compromises GFR. Thus it is well accepted that increase in cytosolic Ca^{2+} content could be an intermediate factor triggering the constriction of GMCs and/or VSMCs for the increase in renal circulation resistance and is responsible for reduced GFR (4, 11, 33).

In the present study, we observed a significant elevation of the Cr level but a marked decrease of GFR in FHF rats caused by GalN/LPS challenge accompanied with significant increase in serum levels of TNF-α and ET-1. This renal insufficiency did not seem to be caused by significant glomerular or tubular damage since it is not supported by renal histopathology and urine albuminuria and NAG levels. A significant increase in mRNA and protein levels for IP_3R1 in renal tissues was

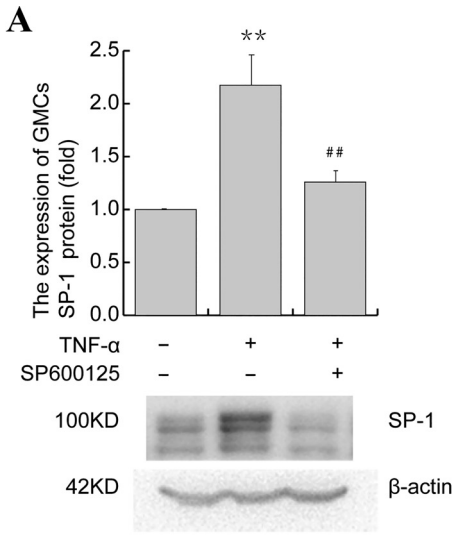

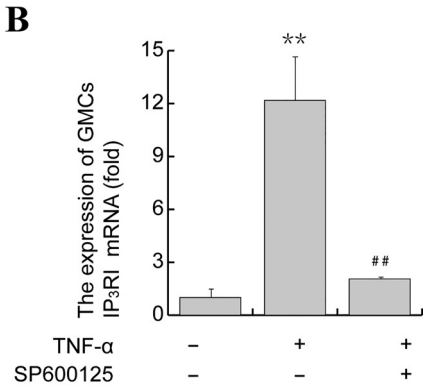

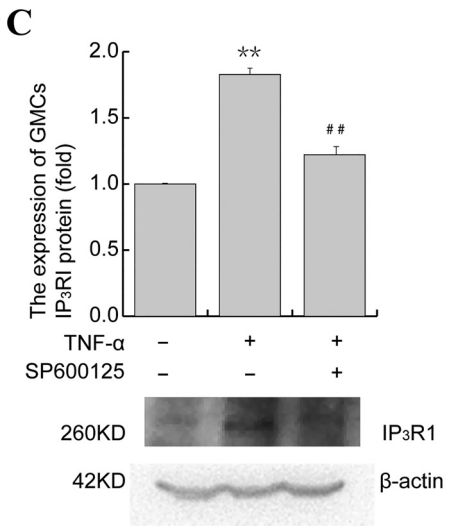

Fig. 8. Effects of JNK inhibitor in IP_3R1 expression induced by TNF-α. *A*: Western blot analysis of changes in SP-1 protein levels after SP600125 treatment. *B*: quantitative results of IP_3R1/GAPDH mRNA ratios relative to the control using qRT-PCR assay. *C*: Western blot analysis of changes in IP_3R1 protein levels after SP600125 treatment. Data represent the means ± SE ($n = 3$).**$P < 0.01$, compared with 0 h or siRNA-NC group. ##$P < 0.01$, compared with siRNA-NC + TNF-α.

accompanied with renal insufficiency in this animal model of renal insufficiency. During the development of FHF in animal model, serum levels of TNF-α and ET-1 and renal dysfunction are manifestations similar to FHF patients in clinical observation. In our previous study, we have demonstrated that TNF-α play a key role during FHF accompanied with AKI (29). PKC-α activation is under the control of TNF-α activity (30). Therefore, *PKC-α* silencing in FHF rats improved the renal function and GFR levels and decreased IP_3R1 mRNA and protein expression levels. The increase in glomerular calcium content and GIS levels was accompanied with FHF rats and silencing *PKC-α* corrected these abnormalities. Thus the findings from our animal model of FHF with renal insufficiency largely support the proposed mechanisms of acute renal dysfunction during severe liver failure (14, 31).

PKC is widely distributed in various tissues and participates in numerous signaling cascades. PKC-α is the major isoform existing in kidneys and plays a very important role in maintaining normal renal function (16). Mesangial cell dilation and constriction are tightly under the control of PKC activation (9). Notably, TNF-α upregulates IP_3R1 expression via two independent signaling pathways (TNFR1/PC-PLC/PKC-α and TNFR2) (30). In the present study, our findings demonstrated that lentivirus-mediated *PKC-α* silence significantly suppressed the elevation of serum creatinine level in rats secondary to FHF, markedly improved GFR, and reduced the expression of IP_3R1 mRNA and protein levels in renal tissues. At the same time, Ca^{2+} levels were reduced in glomeruli from rats receiving injection of lentiviral vector harboring shRNA against *PKC-α*. Therefore, it is our speculation that *PKC-α* silencing reduces intracellular Ca^{2+} release by suppressing IP_3R1 expression in GMCs and VSMCs during FHF and improves GFR through the inhibition of cell contraction and reduction of GIS. In this process, it is most likely that *PKC-α* is an important molecule through which TNF-α upregulates IP_3R1 expression, and it is not surprising that *PKC-α* silencing exhibits a protective effect on renal insufficiency.

To investigate the cellular pathway of IP_3R1 upregulation mediated by the TNF-α−PKC-α pathway, we further explore the molecular signaling mechanisms. TNF-α treatment in GMCs clearly increased the mRNA and protein levels of both PKC-α and IP_3R1, markedly enhanced cellular sensitivity to

ET-1, and elevated intracellular calcium release. Thus RNA interference of PKC-α expression in GMCs significantly abrogated TNF-α-mediated upregulation of IP_3R1 mRNA and protein expression and markedly suppressed ET-1-mediated elevation of Ca^{2+} concentration in TNF-α-treated GMCs.

We hypothesized that TNF-α-stimulated upregulation of IP_3R1 expression may affect *IP₃R1* transcription by increasing the IP_3R1 mRNA level. To test this hypothesis, we used a ChIP technology based on the following understanding. The transcription factor SP-1 is reported to be necessary for TNF-α regulation of IP_3R1 expression in mouse nerve cells (17). However, these events have not yet been investigated in renal cells. Our results revealed that TNF-α treatment resulted in an increase, reaching a peak at 8 h, in SP-1 protein expression, and the phase of increased expression was coincident with that of IP_3R1 mRNA expression. ChIP experiments proved that the strongest binding of SP-1 to the *IP₃R1* promoter occurred during this time frame, suggesting that TNF-α affected the promoter activity by enhancing SP-1 protein expression and promoter binding, subsequently elevating IP_3R1 mRNA levels and further influencing IP_3R1 protein expression. Given the fact that siRNA-PKC-α significantly suppressed TNF-α-stimulated increase of SP-1 protein expression and the binding of SP-1 protein to the *IP₃R1* promoter, it is conceivable that PKC-α affected IP_3R1 expression at a transcriptional level through the SP-1 transcription factor and that the PKC-α-SP-1 route is critical for TNF-α to modulate IP_3R1 expression during renal insufficiency.

Mitogen-activated protein kinase (MAPK) is a serine/threonine protein kinase that is widely distributed in cells. The MAPK family includes ERK, JNK-SAPK, and p38, which are crucial in regulating cell proliferation, differentiation, and gene transcription in response to extracellular signals (20). It is reported that PKC-α regulates expression of both JNK and p-JNK (10, 19). We found a marked elevation of JNK and p-JNK expression in the TNF-α-treated GMCs, and the phase of elevated expression was consistent with the changes of SP-1 levels. *PKC-α* silencing exerted a mild effect on JNK and p-JNK protein levels compared with the siRNA-NC group but did attenuate TNF-α-stimulated increase in JNK and p-JNK protein levels. Pretreatment with SP600125 (JNK inhibitor) suppressed TNF-α-stimulated elevation of SP-1 protein expression and significantly inhibited the downstream increase in IP_3R1 mRNA and protein expression levels. These findings indicate that TNF-α may upregulate JNK/p-JNK expression via PKC-α and JNK might participate in the TNF-α-elicited IP_3R1 expression pathway. The net effect would ultimately change SP-1 protein expression and affect IP_3R1 expression. Taken together, our findings demonstrate that TNF-α upregulates IP_3R1 expression via the JNK/SP-1 pathway (a downstream pathway of PKC-α) in GMCs. However, it remains to be investigated whether TNF-α affects IP_3R1 expression via ERK and p38 from the MAPK family, and how potential interactions of TNF-α with PKC-α and SP-1 take place in the event of acute renal insufficiency during FHF.

In conclusion, the findings in the present study demonstrate that PKC-α silencing improves renal function and GFR, and suggest that TNF-α is critical in the mediation of renal failure during FHF by binding to the *IP₃R1* promoter via the PKC-α/JNK/SP-1 pathway and in turn upregulating IP_3R1 expression at a transcriptional level. Collectively, this study confers concept-proving evidence of a novel molecular intervention by directly targeting the PKC-α/JNK/SP-1 pathway in severe liver failure with renal insufficiency.

ACKNOWLEDGMENTS

We are grateful to Dr. Yuan Liu and Yang Chen (The First Affiliated Hospital, China Medical University) for technical assistance in microscope and fluorescence examination. We are also grateful to Dr. Dong-Liang Man (The First Affiliated Hospital, China Medical University) for serum biochemical analysis and the comments to this manuscript.

Present address of J. Wu: Key Laboratory of Molecular Virology, Fudan Univ. Shanghai Medical College, 138 Yixue Yuan Rd., P. O. Box 228, Shanghai 200032, China (e-mail: jian.wu@fudan.edu.cn).

GRANTS

This work is supported by the National Natural Science Foundation of China Grants 30270607 (to P. Liu) and 81272436 and 81572356 (to J. Wu) and Ministry of Science and Technology Grant 2016YFE0107400 (to J. Wu).

DISCLOSURES

No conflicts of interest, financial or otherwise, are declared by the authors.

AUTHOR CONTRIBUTIONS

D.-L.W., W.-Y.D., W.W., Y.W., Y.Z., Y.-T.Z., and J.W. performed experiments; D.-L.W., W.-Y.D., W.W., Y.W., Y.Z., Y.-T.Z., and J.W. analyzed data; D.-L.W., W.-Y.D., Y.W., Y.Z., Y.-T.Z., J.W., and P.L. interpreted results of experiments; D.-L.W. and J.W. drafted manuscript; D.-L.W., J.W., and P.L. edited and revised manuscript; J.W. and P.L. approved final version of manuscript.

REFERENCES

1. **Akriviadis E, Botla R, Briggs W, Han S, Reynolds T, Shakil O.** Pentoxifylline improves short-term survival in severe acute alcoholic hepatitis: a double-blind, placebo-controlled trial. *Gastroenterology* 119: 1637–1648, 2000. doi:10.1053/gast.2000.20189.
2. **Andresen BT, Jackson EK, Romero GG.** Angiotensin II signaling to phospholipase D in renal microvascular smooth muscle cells in SHR. *Hypertension* 37: 635–639, 2001. doi:10.1161/01.HYP.37.2.635.
3. **Arroyo V, Fernandez J, Ginès P.** Pathogenesis and treatment of hepatorenal syndrome. *Semin Liver Dis* 28: 81–95, 2008. doi:10.1055/s-2008-1040323.
4. **Brightling C, Berry M, Amrani Y.** Targeting TNF-alpha: a novel therapeutic approach for asthma. *J Allergy Clin Immunol* 121: 5–10, 2008. doi:10.1016/j.jaci.2007.10.028.
5. **Cunningham PN, Wang Y, Guo R, He G, Quigg RJ.** Role of Toll-like receptor 4 in endotoxin-induced acute renal failure. *J Immunol* 172: 2629–2635, 2004. doi:10.4049/jimmunol.172.4.2629.
6. **Fellner SK, Arendshorst WJ.** Angiotensin II Ca^{2+} signaling in rat afferent arterioles: stimulation of cyclic ADP ribose and IP3 pathways. *Am J Physiol Renal Physiol* 288: F785–F791, 2005. doi:10.1152/ajprenal.00372.2004.
7. **Fuller AJ, Hauschild BC, Gonzalez-Villalobos R, Awayda MS, Imig JD, Inscho EW, Navar LG.** Calcium and chloride channel activation by angiotensin II-AT_1 receptors in preglomerular vascular smooth muscle cells. *Am J Physiol Renal Physiol* 289: F760–F767, 2005. doi:10.1152/ajprenal.00422.2004.
8. **Ginès P, Guevara M, Arroyo V, Rodés J.** Hepatorenal syndrome. *Lancet* 362: 1819–1827, 2003. doi:10.1016/S0140-6736(03)14903-3.
9. **Jin JS, Yao CW, Ka SM, Chin TY, Chueh SH, Lee HS, Sheu LF, Lin YF, Lee WH, Chen A.** IgA immune complex blunts the contraction of cultured mesangial cells through the inhibition of protein kinase C and intracellular calcium. *Chin J Physiol* 47: 79–87, 2004.
10. **Jin M, Ande A, Kumar A, Kumar S.** Regulation of cytochrome P450 2e1 expression by ethanol: role of oxidative stress-mediated pkc/jnk/sp1 pathway. *Cell Death Dis* 4: e554, 2013. doi:10.1038/cddis.2013.78.
11. **Jurkovicova D, Sedlakova B, Lacinova L, Kopacek J, Sulova Z, Sedlak J, Krizanova O.** Hypoxia differently modulates gene expression of inositol 1,4,5-trisphosphate receptors in mouse kidney and HEK 293 cell line. *Ann N Y Acad Sci* 1148: 421–427, 2008. doi:10.1196/annals.1410.034.

12. **Liu Y, Lu S, Zhang Y, Wang X, Kong F, Liu Y, Peng L, Fu Y.** Role of caveolae in high glucose and TGF-β_1 induced fibronectin production in rat mesangial cells. *Int J Clin Exp Pathol* 7: 8381–8390, 2014.
13. **Moore JK, Love E, Craig DG, Hayes PC, Simpson KJ.** Acute kidney injury in acute liver failure: a review. *Expert Rev Gastroenterol Hepatol* 7: 701–712, 2013. doi:10.1586/17474124.2013.837264.
14. **Moreau R, Lebrec D.** Acute kidney injury: new concepts. Hepatorenal syndrome: the role of vasopressors. *Nephron, Physiol* 109: 73–79, 2008. doi:10.1159/000142939.
15. **Natarajan SK, Basivireddy J, Ramachandran A, Thomas S, Ramamoorthy P, Pulimood AB, Jacob M, Balasubramanian KA.** Renal damage in experimentally-induced cirrhosis in rats: Role of oxygen free radicals. *Hepatology* 43: 1248–1256, 2006. doi:10.1002/hep.21179.
16. **Ostlund E, Mendez CF, Jacobsson G, Fryckstedt J, Meister B, Aperia A.** Expression of protein kinase C isoforms in renal tissue. *Kidney Int* 47: 766–773, 1995. doi:10.1038/ki.1995.117.
17. **Park KM, Yule DI, Bowers WJ.** Tumor necrosis factor-alpha-mediated regulation of the inositol 1,4,5-trisphosphate receptor promoter. *J Biol Chem* 284: 27557–27566, 2009. doi:10.1074/jbc.M109.034504.
18. **Qi Z, Whitt I, Mehta A, Jin J, Zhao M, Harris RC, Fogo AB, Breyer MD.** Serial determination of glomerular filtration rate in conscious mice using FITC-inulin clearance. *Am J Physiol Renal Physiol* 286: F590–F596, 2004. doi:10.1152/ajprenal.00324.2003.
19. **Saberi B, Ybanez MD, Johnson HS, Gaarde WA, Han D, Kaplowitz N.** Protein kinase C (PKC) participates in acetaminophen hepatotoxicity through c-jun-N-terminal kinase (JNK)-dependent and -independent signaling pathways. *Hepatology* 59: 1543–1554, 2014. doi:10.1002/hep.26625.
20. **Safirstein R.** Renal stress response and acute renal failure. *Adv Ren Replace Ther* 4, *Suppl* 1: 38–42, 1997.
21. **Saleem H, Tovey SC, Rahman T, Riley AM, Potter BV, Taylor CW.** Stimulation of inositol 1,4,5-trisphosphate (IP3) receptor subtypes by analogues of IP3. *PLoS One* 8: e54877, 2013. doi:10.1371/journal.pone.0054877.
22. **Schlöndorff D.** Roles of the mesangium in glomerular function. *Kidney Int* 49: 1583–1585, 1996. doi:10.1038/ki.1996.229.
23. **Schroeder AC, Imig JD, LeBlanc EA, Pham BT, Pollock DM, Inscho EW.** Endothelin-mediated calcium signaling in preglomerular smooth muscle cells. *Hypertension* 35: 280–286, 2000. doi:10.1161/01.HYP.35.1.280.
24. **Shankar A, Loizidou M, Burnstock G, Taylor I.** Noradrenaline improves the tumour to normal blood flow ratio and drug delivery in a model of liver metastases. *Br J Surg* 86: 453–457, 1999. doi:10.1046/j.1365-2168.1999.01045.x.
25. **Svotelis A, Gévry N, Gaudreau L.** Chromatin immunoprecipitation in mammalian cells. *Methods Mol Biol* 543: 243–251, 2009. doi:10.1007/978-1-60327-015-1_16.
26. **Szczepańska-Konkel M, Jankowski M, Stiepanow-Trzeciak A, Angielski S.** Effects of diadenosine polyphosphates on glomerular volume. *Br J Pharmacol* 144: 1109–1117, 2005. doi:10.1038/sj.bjp.0706149.
27. **Udagawa T, Hanaoka K, Kawamura M, Hosoya T.** Characteristics of spontaneous calcium oscillations in renal tubular epithelial cells. *Clin Exp Nephrol* 16: 389–398, 2012. doi:10.1007/s10157-012-0588-4.
28. **van Bemmelen MX, Szczepańska-Konkel M, Jastorff B, Jankowski M, Angielski S.** Effect of cAMP analogues on glomerular inulin space of isolated rats renal glomeruli. *J Physiol Pharmacol* 56: 111–120, 2005.
29. **Wang JB, Wang DL, Wang HT, Wang ZH, Wen Y, Sun CM, Zhao YT, Wu J, Liu P.** Tumor necrosis factor-alpha-induced reduction of glomerular filtration rate in rats with fulminant hepatic failure. *Lab Invest* 94: 740–751, 2014. doi:10.1038/labinvest.2014.71.
30. **Wang YR, Li ZG, Fu JL, Wang ZH, Wen Y, Liu P.** TNFα-induced IP3R1 expression through TNFR1/PC-PLC/PKCα and TNFR2 signalling pathways in human mesangial cell. *Nephrol Dial Transplant* 26: 75–83, 2011. doi:10.1093/ndt/gfq406.
31. **Wong F.** Recent advances in our understanding of hepatorenal syndrome. *Nat Rev Gastroenterol Hepatol* 9: 382–391, 2012. doi:10.1038/nrgastro.2012.96.
32. **Woodcock EA, Matkovich SJ.** Ins(1,4,5)P3 receptors and inositol phosphates in the heart-evolutionary artefacts or active signal transducers? *Pharmacol Ther* 107: 240–251, 2005. doi:10.1016/j.pharmthera.2005.04.002.
33. **Yamada J, Ohkusa T, Nao T, Ueyama T, Yano M, Kobayashi S, Hamano K, Esato K, Matsuzaki M.** [Up-regulation of inositol 1, 4, 5-trisphosphate receptor expression in atrial tissue in patients with chronic atrial fibrillation]. *J Cardiol* 39: 57–58, 2002.